MATERIALS SCIENCE

Deviating from the pure MAX phase concept: Radiation-tolerant nanostructured dual-phase Cr_2AlC

M. A. Tunes[1]*, M. Imtyazuddin[2]*, C. Kainz[3], S. Pogatscher[1], V.M. Vishnyakov[2]

A dual-phase Cr_2AlC material was synthesized using magnetron sputtering at a temperature of 648 K. A stoichiometric and nanocrystalline MAX phase matrix was observed along with the presence of spherical-shaped amorphous nano-zones as a secondary phase. The irradiation resistance of the material was assessed using a 300-keV Xe ion beam in situ within a transmission electron microscope up to 40 displacements per atom at 623 K: a condition that extrapolates the harmful environments of future fusion and fission nuclear reactors. At the maximum dose investigated, complete amorphization was not observed. Scanning transmission electron microscopy coupled with energy-dispersive x-ray revealed an association between swelling due to inert gas bubble nucleation and growth and radiation-induced segregation and clustering. Counterintuitively, the findings suggest that preexisting amorphous nano-zones can be beneficial to Cr_2AlC MAX phase under extreme environments.

INTRODUCTION

Mainly motivated by the intense progress of energy industry and the space race in the second half of the 20th century, intense efforts were devoted into the design techniques for the synthesis of new structural materials. The progress has demanded that these materials can resist extreme environments, such as fusion and fission reactors, supersonic aircraft flights, and high forces exhibited on structural spacecraft and rocket components. On the wide range of developed techniques, reactive hot pressing (RHP) (*1*) allowed the synthesis and densification of new classes of refractory carbides and nitrides, which later demonstrated a set of properties for suitable application at high temperatures when compared with the well-known sintered-based ceramic materials. Among these materials, the combination between an early transition metal (M) and an element from the groups 13 or 14 (A) with C or N (X) laid the foundations for the discovery of the so-called $M_{n+1}AX_n$ phases (or simply MAX phases).

Primarily designed and engineered around the 1960s (*2*) and revisited in the 1990s (*3*, *4*), MAX phases comprise a unique class of materials that are distinct from either conventional multicomponent carbides or nitrides. They were already observed to combine metal-like plastic deformation properties with high hardness and high ductility (*3*), nano-layered microstructure (*5*), and potential for enhanced corrosion and oxidation resistances at room and high temperatures (*6*–*8*). From an atomistic point of view, MAX phases are of a specific hexagonal crystal structure with C or N atoms within the interstitial positions of an octahedral M_6X unit cell with the layers of A atoms at the center of the interatomic spaces of M atoms (*3*). With respect to their thermodynamic stability and melting point, it has been reported that MAX phases, such as the Ti_3SiC_2, can be stable in inert atmospheres up to 1973 K, although unstable above 1673 K under atmospheric conditions (*9*). In addition, early reports from Nowotny and co-worker (*2*)—apud Barsoum (*9*)—claim that the latter phase dissociates at 1973 K into TiC and a liquid phase, thus pointing that MAX phases may not have a defined melting temperature. Although MAX phases can be quite machinable, several reports indicate a challenge of producing a fully pure stoichiometric phase in their bulk form when using RHP or a similar method (*4*, *10*, *11*). Notwithstanding belonging to an entire new class of materials with interesting properties, since their discovery, MAX phases are still pending of market consolidation and commercialization as a functional material (*12*).

A promising field for integration of MAX phases as structural materials is nuclear technology. In this niche of materials science, the materials' response to energetic particle irradiation is a major concern as it can induce severe degradation by modifying their initial properties. Strict engineering criteria and safety regulations treat any modification on the initial materials properties as damage and degradation. Recently, Wang *et al.* (*13*) compiled a comprehensive review on the effects of energetic particle irradiation on MAX phases. The authors concluded that, given the inherent wide chemical diversity of the MAX phase family as well as the broad irradiation conditions and diversity of phases reported in literature, more research is required to understand the microstructural evolution and predicted behavior of such materials under irradiation.

Early reports on the neutron irradiation response have been limited to bulk Ti-based MAX phases, where a high phase stability up to doses around 3 displacements per atom (dpa) with suppressed nucleation and growth of extended crystalline defects for irradiation temperatures up to 968 K was found (*14*–*16*). Neutron irradiations carried out at the high-flux isotope reactor at 1273 K up to 10 dpa—which, up to date, is the maximum neutron dose analyzed for MAX phases—have shown that Ti-based MAX phases can experience radiation-induced segregation with concurrent matrix phase decomposition (*17*). Heavy ion irradiation has also been used as an important alternative to investigate the deleterious effects of irradiations in Ti-based MAX phases, and most of the reports demonstrate enormous potential for MAX phases in nuclear reactors (*18*–*21*). An important result on the radiation response of MAX phases has been first provided by Whittle *et al.* (*19*), who analyzed the behavior of Ti-based MAX phases with heavy ion irradiation in situ transmission electron microscopy (TEM). The authors detected and confirmed that such materials can retain crystallinity at severely high Xe doses. The absence of matrix phase amorphization under

[1]Chair of Nonferrous Metallurgy, Montanuniversitaet Leoben, Leoben, Austria. [2]Institute for Materials Research, University of Huddersfield, Huddersfield, UK. [3]Christian Doppler Laboratory for Advanced Coated Cutting Tools, Department of Materials Science, Montanuniversitaet Leoben, Leoben, Austria.
*Corresponding author. Email: m.a.tunes@physics.org (M.A.T.); mohammed.imtyazuddin@hud.ac.uk (M.I.)

irradiation is a preliminary confirmation that such materials are of superior radiation tolerance when compared with conventional sintered ceramics that often incur amorphization at much lower damage doses (*22*). However, instabilities in Ti-based MAX phases under proton irradiation recently concluded that these materials may have limited applicability in high-temperature reactors (*23*, *24*).

Although the carbide MAX phases comprise an entire class of materials, the final properties of a specific phase will be dependent on the base element (M). An alternative to Ti-based MAX phases has been to explore ternary carbides within the Cr-Al-C system. The Cr_2AlC MAX phase has a few important advantages: It can be produced at relatively low temperatures (*25*), and also, the material can be first deposited in amorphous form then crystallized in air without any deterioration (*26*). The possibility of producing single-phase coatings of Cr_2AlC MAX phase could soon revolutionize the field of coatings for nuclear fuel cladding systems such as Zr-based alloys, which suffer from oxidation at high temperatures. This was the main cause for the Fukushima-Daiichi nuclear disaster in 2011, and existing solutions such as titanium nitride (TiN) thin films have been shown to strongly dissociate and degrade in severe energetic irradiation environments (*27*). The Cr_2AlC alternative also arises because the element Cr has been historically studied because of its suitable high-temperature corrosion and oxidation resistances (*6*). Therefore, a Cr-based MAX phase will be indicated for such nuclear applications, provided the demonstration of its superior radiation resistance against existing solutions such as TiN or high-entropy alloy thin films (*27*, *28*). It is worth emphasizing that the corrosion/oxidation behavior of Cr_2AlC has been recently assessed under simulated light-water reactor (LWR) conditions, and it outperformed the Ti-based MAX phase counterparts (*29*).

Radiation studies on Cr_2AlC MAX phase are limited to date and have been mostly investigated at room and moderate temperatures (*30*–*35*). Irradiation of Cr_2AlC MAX phase processed by spark plasma sintering with 7-MeV Xe^{26+} and 500-keV He^{2+} at 300 K have shown retained crystallinity in doses up to 1 dpa, and notable alterations to their initial mechanical properties were observed (*32*). In other studies of magnetron-sputtered Cr_2AlC thin films with fluences in the range of 10^{14} to 10^{15} Xe^{2+} ions cm^{-2}, the MAX phases partially amorphized at 2.2 dpa via a transformation from Cr_2AlC MAX phase to the intermediary $(Cr,Al)_2C_x$ phase (known as γ phase), finally resulting in the amorphous state (*33*, *34*). Complete amorphization was observed at 6.2 dpa when irradiation is carried out at room temperature (*34*). In a recent work on the radiation response of magnetron-sputtered Cr_2AlC MAX phase at room and high temperatures up to fluences of 2.1×10^{16} Xe^{+} ions cm^{-2} (90 dpa), amorphization at room temperature was confirmed. However, outstanding resistance to amorphization in irradiations performed at 650 K up to 90 dpa was observed (*30*). This high radiation resistance at high temperature was believed to be due to the nanocrystalline nature of Cr_2AlC MAX phase, which prevents transformation to γ phase. Most recently, deviations from ideal Cr_2AlC stoichiometry were accounted for the formation of chromium aluminides (Cr_5Al_8) along with the Cr_2AlC MAX phase and enhanced nanocrystallinity of thin films, resulting in higher phase stability up to 138 dpa under heavy ion irradiation (*36*).

So far, it is possible to state that the Cr_2AlC MAX phase has a very broad processing window when produced by physical vapor deposition (for instance, magnetron sputtering). Three major phases compete to nucleate and grow within the Cr-Al-C system: the stoichiometric Cr_2AlC, the γ phase, and the amorphous phase; the first seems to be thermodynamically preferential. The question remains as to how the material would behave under irradiation if it is not fully crystalline after deposition and, in addition, what are the fundamental processes behind the radiation resistance of the Cr_2AlC.

Here, we deviate from the pure MAX phase concept by synthesizing a dual-phase material with the Cr_2AlC MAX phase as matrix and an amorphous phase of the same local chemistry, as the secondary phase. Following a detailed electron microscopy characterization, the as-deposited specimens were subjected to ion irradiation with 300-keV Xe^{+} in situ within a TEM at 623 K up to 40 dpa peak. Here, postirradiation characterization unveiled new radiation resistance mechanisms of Cr_2AlC MAX phase, which manifest synergistically due to the nanocrystallinity and the reported presence of the amorphous nano-zones within the coating microstructure. It will be demonstrated that such amorphous nano-zones provide additional resistance to complete amorphization of the material as the irradiation evolves to higher doses, which unexpectedly opposes to previously reported phenomena on conventional and nuclear-grade ceramics. The results pave the way for considering the use of amorphous materials within the research scope of nuclear materials, especially on coatings for accident tolerant fuels.

RESULTS

Cr_2AlC synthesis and morphology

A detailed scanning TEM (STEM) and energy-dispersive x-ray (EDX) microstructural characterization of the Cr_2AlC as deposited is shown in Fig. 1. Low-magnification high-angle annular dark-field (HAADF) imaging and bright-field (BF) micrographs in Fig. 1 (A and B, respectively) indicate that the microstructure is composed of columnar-like nano-grains with sizes around 30 to 50 nm. EDX analysis at high magnification in Fig. 1 (C to H) shows that the Cr, Al, and C are uniformly distributed over the thin film profile. As shown in Table 1, the measured composition of the as-deposited film matches the expected stoichiometry for pure Cr_2AlC MAX phase.

Nanocrystallinity and amorphous nano-zones

TEM characterization of the Cr_2AlC as-deposited thin film is shown in Fig. 2. The combination of bright-field TEM (BFTEM) and selected-area diffraction pattern (SAED) (Fig. 2, A and B, respectively) indicates that the film is nanocrystalline. The presence of a central amorphous ring in the SAED diffraction pattern in Fig. 2B was further investigated with high-resolution TEM (HRTEM). The HRTEM micrograph in Fig. 2C shows the presence of circular-shaped amorphous nano-regions within the Cr_2AlC matrix phase. Such amorphous nano-zones were also investigated in high-magnification STEM-EDX as shown in the set of Fig. 2 (E to I), indicating that, qualitatively at least, they share the same composition as the matrix (as shown within the yellow circles).

Crystallographic structure

Figure 2J shows the grazing incidence x-ray diffraction of the coating in its as-deposited state. At least two major findings must be commented. First, the material is crystalline. It was shown earlier that narrow, well-defined peaks can only be obtained within a fully crystallized material (*26*). The presence of crystalline hexagonal Cr_2AlC is clearly evident from the diffraction pattern of the as-deposited coating as indexed using crystallographic data from

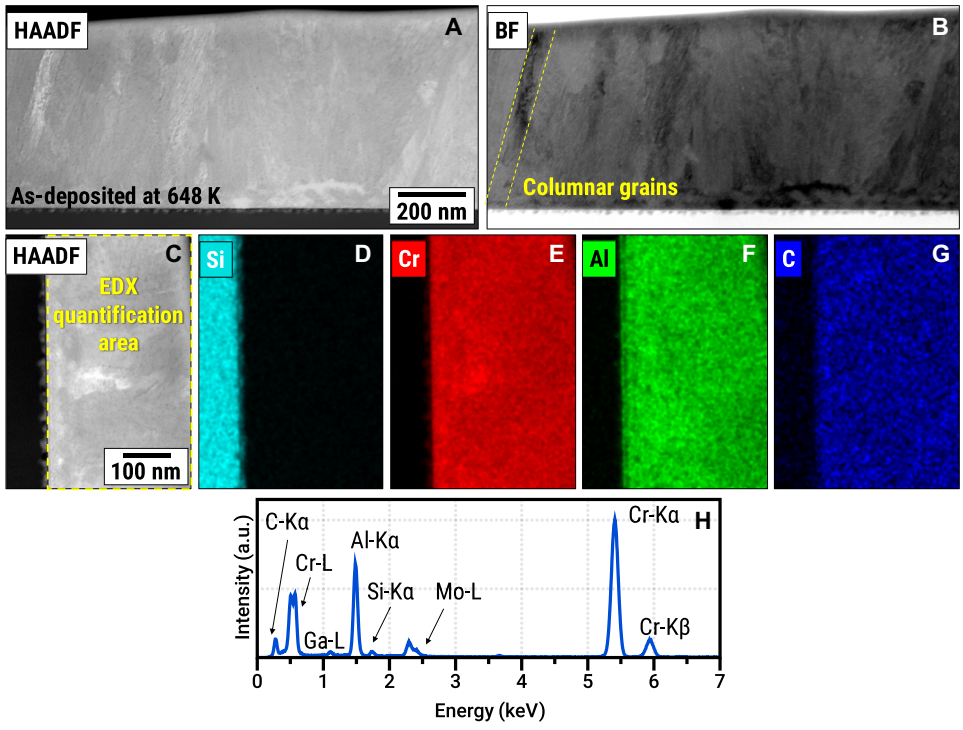

Fig. 1. Nanocrystalline Cr_2AlC MAX phase as deposited at 648 K. A columnar-like microstructure is observed after deposition at 648 K with a high degree of nanocrystallinity as observed in the HAADF (**A**) and BF (**B**) micrographs. Elemental quantification shown in Table 1 demonstrated that correct 211 MAX phase stoichiometry could be achieved. Note that the EDX map in (**D** to **G**) was taken from the area indicated in the HAADF micrograph in (**C**). Panel (H) shows the EDX spectrum of the analyzed area denoted in (C). a.u., arbitrary units.

Table 1. Elemental composition of Cr_2AlC. The composition of pristine Cr_2AlC thin films as measured using EDX in a field-emission gun scanning electron microscope (FEG-SEM). In addition, the composition of the films was measured in a STEM-EDX at three different conditions: matrix as deposited at 648 K, matrix irradiated up to 40 dpa at 623 K, and along the GBs up to 40 dpa at 623 K. Note that results were quantified in atomic %.

Elements (expected pristine atomic composition)	Matrix phase			Grain boundaries
	As deposited at 648 K (FEG-SEM-EDX)	As deposited at 648 K (STEM-EDX)	Irradiated up to 40 dpa at 623 K (STEM-EDX)	Irradiated up to 40 dpa at 623 K (STEM-EDX)
Cr (50)	53.2 ± 2.7	48.9 ± 10.6	49.0 ± 10.3	51.5 ± 10.7
Al (25)	23.4 ± 1.2	29.7 ± 7.8	30.2 ± 7.8	26.2 ± 6.7
C (25)	23.4 ± 1.2	21.4 ± 3.7	17.9 ± 3.0	19.0 ± 3.1
Xe (0)	–	–	2.9 ± 0.6	3.3 ± 0.6

literature (*37*). The a and c lattice parameters amount to 2.83 and 12.87 Å, respectively, resulting in a c/a ratio of 4.55. This observation confirms the formation of hexagonal MAX phase Cr_2AlC and the absence of trigonal distorted $(Cr,Al)_2C_x$. Second, the background in the x-ray diffraction (XRD) pattern is high, which can be an indication of amorphous phase presence. Moreover, the characteristic 002 and 004 basal plane peaks are lacking, and the 006 reflection overlaps with the dominant 103 peak. The reflections are furthermore low in intensity and display a large peak broadening, as typical for nanocrystalline materials.

Heavy ion irradiations

The Cr_2AlC as-deposited thin film was subjected to heavy ion irradiations using a 300-keV Xe^+ ion beam in situ within a TEM at 623 K, a temperature of relevance for most commercial nuclear reactors operating under normal conditions. The microstructural evolution of the Cr_2AlC thin film as a function of the irradiated dose is shown in the set of BFTEM micrographs in Fig. 3 (A to D). By monitoring the diffraction pattern of the area under investigation during the irradiation experiments, it can be noticed in the micrograph in Fig. 3H that the film preserved its crystal structure at a very high dose of 40 dpa. There is no visible redistribution of diffracted electron intensity between crystalline (diffraction spots) and amorphous (diffraction rings) diffractions. This allows to conclude that, at this dose, no complete amorphization has taken place. It is worth emphasizing that the presence of the amorphous rings in the SAED patterns in Fig. 3 (E to G) can be attributed to the presence of the amorphous nano-zones in the pristine material (i.e., 0 dpa) as shown in Fig. 2. In the BFTEM micrograph in Fig. 3D, it is noticeable that the TEM contrast along the grain boundaries (GBs) has

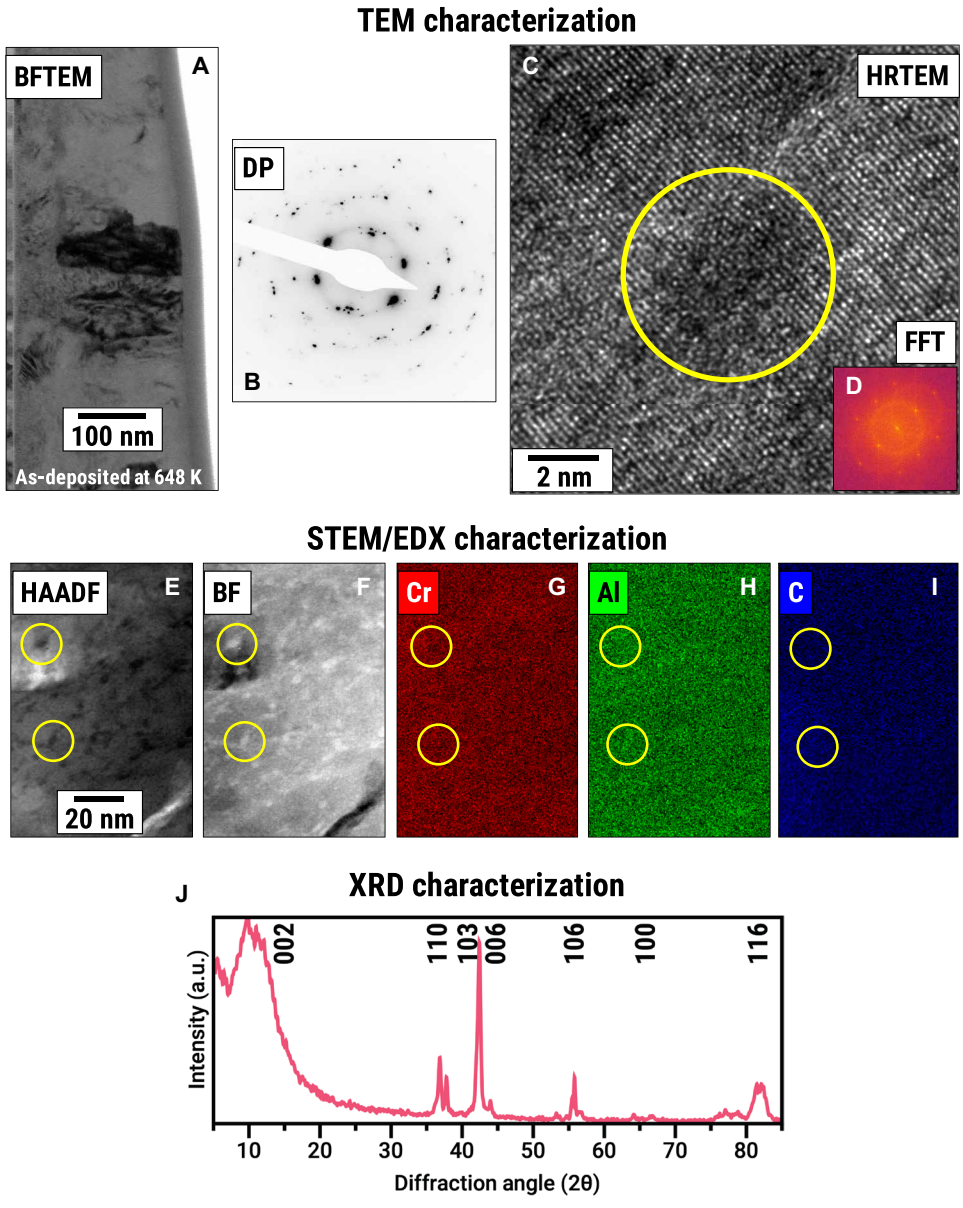

Fig. 2. Amorphous nano-zones in the Cr_2AlC thin films as deposited at 648 K. The deposited Cr_2AlC MAX phase thin film exhibited the presence of amorphous nano-zones in its matrix microstructure (**A** to **D**); however, qualitative STEM-EDX characterization (**E** to **I**) revealed that such amorphous nano-zones have the closer elemental composition to the matrix phase. HRTEM reveals that the amorphous nano-zones are regions where the Cr_2AlC crystal structure is disrupted as shown in micrograph (C). SAED pattern (B) and fast Fourier transforms (FFTs) from HRTEM micrographs (C) and (D) confirm these amorphous zones as they generate characteristic rings. TEM and STEM-EDX results were cross-checked using XRD characterization (**J**), which confirmed a low degree of crystallinity in the investigated material and thus indicates the presence of amorphous material. Note that the FFT in (D) was generated using the whole HRTEM micrograph in (C).

significantly changed from 0 to 40 dpa. Dark thick lines are now observed along the GBs, which can be attributed to an increase in mass thickness.

Postirradiation characterization

As can be seen from Table 1, the overall composition of the film irradiated to 40 dpa has not changed significantly when compared to as-deposited thin films. Figure 4 shows segregation of Xe bubbles preferentially at the GBs (Fig. 4, C and G), which has motivated the study of such microstructure at higher magnifications within the STEM. A more detailed characterization of Xe bubbles after 40 dpa of heavy ion irradiation is shown in Fig. 5. The composite EDX profiles for both Cr and Al along the GB and within the matrix are exhibited in Fig. 5 (A and C, respectively). It is clear that Cr segregates at the GBs and that the Xe bubbles are larger along the GBs when compared with the matrix bubbles as shown in Fig. 5 (B and D). Such Cr segregation is linked with the detected "dealumination" of the GB (as shown in Figs. 4, C and G, and 5A), that is, Cr tends to segregate along the GBs while Al tends to deplete at these interfaces, suggesting a transgranular flux of Al in the face of an intragranular flux of Cr. The quantification of Xe bubble sizes in the form of histograms as shown in Fig. 5 (E and F) also corroborates the results.

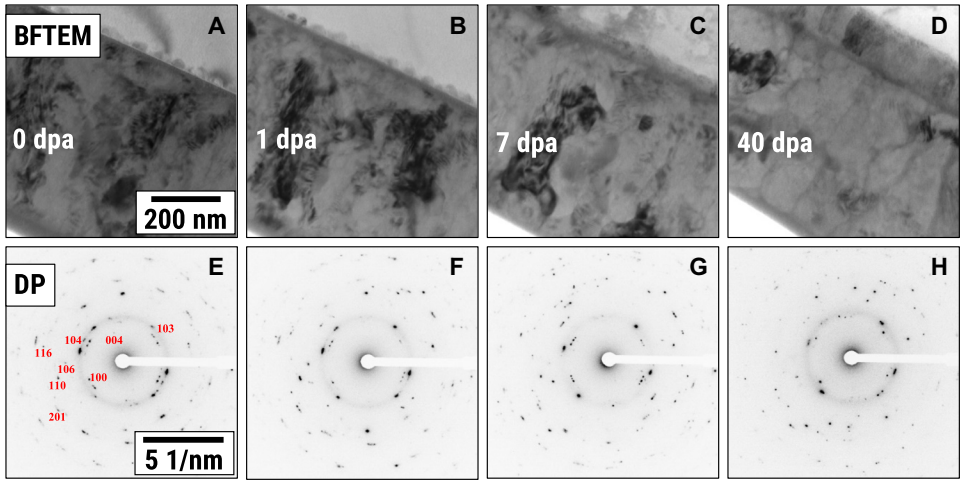

Fig. 3. Heavy ion irradiation with in situ TEM. As can be directly observed, the in situ TEM evolution of the Cr_2AlC MAX phase under extreme irradiation reveals no significant crystalline changes, apart from the thickening of the GBs at doses around 40 dpa. Micrographs (**A** to **D**) and (**E** to **H**) are BFTEM and SAED patterns, respectively, acquired as function of the irradiation dose.

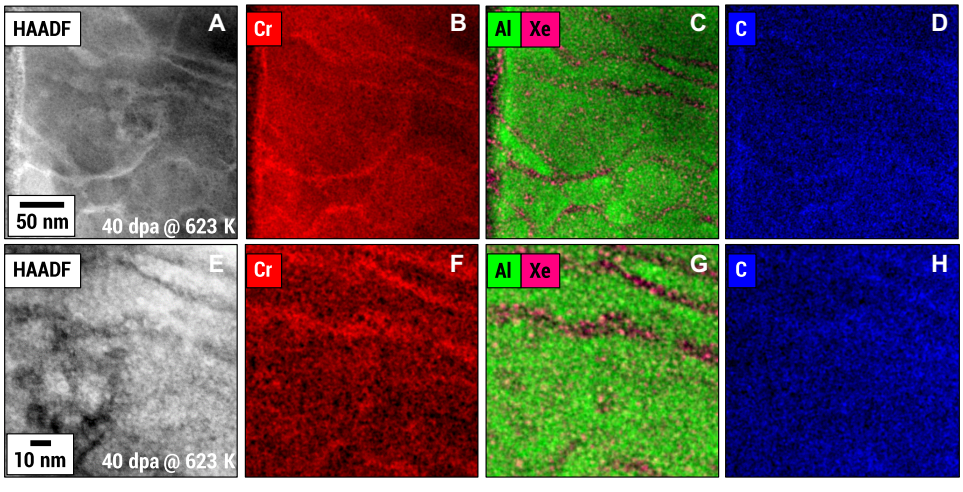

Fig. 4. Dealumination of the Cr_2AlC MAX phase at high doses. The GBs of the matrix phase were observed to suffer dealumination at high doses with concurrent in-segregation of Cr. The HAADF micrograph in (**A**) and its respective STEM-EDX maps (**B** to **D**) show the Cr segregation along the nanocrystalline GBs. This can be observed in detail at a higher magnification in micrographs (**E** to **H**). The presence of Xe bubbles is noted in the STEM-EDX maps (C) and (G).

Figure 6 shows a set of BF, low-angle annular dark-field (ADF), and HAADF micrographs of the material after irradiation up to 40 dpa. It is evident that the nanocrystallinity was preserved after these high-dose irradiations.

Nano-impact testing

Nano-impact testing was used to assess whether the amorphous nano-zones can negatively affect the mechanical response of the produced Cr_2AlC coating under dynamic loading conditions. Figure 7 exhibits a secondary electron micrograph taken in a scanning electron microscope after the test: It is noticeable that the material had not undergone catastrophic failure, and no localized fracture was observed in the material as it has been reported to occur in other systems such as TiFeN (*38*) and CrN (*39*). As noted in Fig. 7, the surface of the dual-phase Cr_2AlC clearly exhibits typical indentation behavior attributed to ductile materials (*40*). The zones surrounding the indenter mark indicate that the material suffered plastic deformation.

DISCUSSION

Microstructural features and the presence of amorphous nano-regions in Cr_2AlC MAX phase thin films

Walter *et al.* (*25*) claimed a required deposition temperature of 723 K for attaining full crystalline Cr_2AlC MAX phase, whereas Li *et al.* (*41*) observed crystalline Cr_2AlC already at 643 K. At lower deposition temperatures, the amorphous phase is observed to be dominant. Thus, the used deposition temperature of 648 K here is in the lower range when aiming for purely crystalline hexagonal Cr_2AlC coatings. While the x-ray diffractogram of the as-deposited coating clearly shows the contribution of crystalline hexagonal Cr_2AlC, the weak signal intensity indicates that the crystallization has not been completed at the applied deposition temperature. The absence of the 002 basal plane reflection in the diffractograms additionally supports this assumption. Abdulkadhim *et al.* (*42*) have shown that the basal peak is only observed at an advanced stage of Cr_2AlC coating crystallization.

Micrographs in Fig. 1 (A and B) demonstrate that the produced film is nanocrystalline with a columnar structure. In this work, the

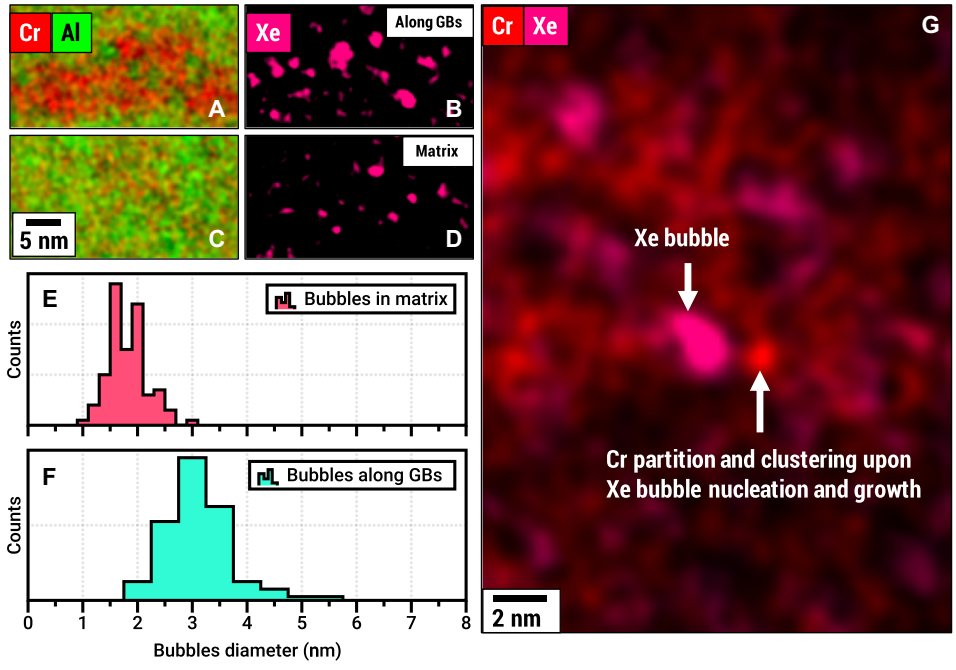

Fig. 5. Unveiling mechanisms of radiation resistance in nanostructured Cr_2AlC MAX phase. Postirradiation STEM-EDX screening at high magnification revealed that the Cr segregation process is mediated by the swelling promoted by nucleation and growth of Xe bubbles. Cr partition and clustering occur at regions closer to Xe bubbles as can be observed in the STEM-EDX maps along a GB (**A** to **D**) and transgranular as shown in (**G**). Bigger Xe bubbles along the nano-GBs (**F**) when compared with bubbles in the matrix (**E**) also suggest that these interfaces are preferential sinks for radiation-induced defects.

SAED patterns were indexed with (004), (100), (103), (104), (106), (110), (116), and (201) reflections using reference data (*43*), thus confirming the presence of Cr_2AlC MAX phase in the produced films. However, the produced film cannot be considered "pure" MAX phase; the micrographs show the presence of amorphous nano-zones transgranularly distributed within the columnar nanograins, which agrees with the observations from XRD. These amorphous nano-zones were characterized both via the identification of amorphous rings in the SAED patterns and using HRTEM and STEM-EDX. The latter indicates that the amorphous nano-zones are of the same stoichiometry of the crystalline Cr_2AlC phase. In this way, the thin film is a dual-phase material, although the amorphous nano-zones were observed to have a similar composition as its Cr_2AlC matrix.

Reference data from literature indicate that, under conventional RHP conditions, Cr_2AlC MAX phase can be synthesized in the temperature range of 1123 to 1723 K. Only above 1523 K that the material can be considered a complete pure Cr2AlC MAX phase, i.e., without the presence of undesired intermetallic and/or other carbide phases (*44*). To the best of our knowledge, apart from secondary intermetallics or carbide phases, the existence of amorphous zones in the Cr_2AlC MAX phase has not been reported yet. The substrate temperature, 648 K, in which the Cr_2AlC MAX phase thin films were produced in this work is (significantly) lower than 1523 K. This poses the natural question why thin solid films of MAX phase materials can be produced using magnetron-sputtering deposition at such low temperatures when compared with other synthesis routes such as RHP.

Sputter deposition of hard thin films differs from RHP or other bulk synthesis methods by its distinct fundamental physical mechanisms governing the formation of the final material. In the former, a low-energy ion beam is often used to sputter atoms from pure elemental targets, and then a flux of ions with the coating constituents is directed toward a substrate in a narrow set of directions. The first explanation why the Cr_2AlC MAX phase can be synthesized at lower temperatures when compared with bulk synthesis processes lies on the fact that such physical-sputtering processes create preferential solid-state diffusion paths throughout the whole thickness of the growing film as the ratio between activation energies for surface, GB, and bulk diffusion is reported to be 1:2:4 (*45*). The latter consideration implies that the substrate where the film will be grown does not require to be held at a high temperature (as compared with other bulk synthesis methods) as solid-state diffusion (consequently crystallization phenomena) has driving force to take place.

Another important consideration is the nanocrystallinity and columnar microstructure of the synthesized films here. Assuming as melting point (T_m) the reported dissociation temperature of Cr_2AlC MAX phase of 1723 K (*46*), the deposition reported in this work was carried out at a homologous temperature of approximately 0.38 T_m. This categorizes our deposition conditions in the middle of the temperature range of zone 2 ($0.3 < T_m < 0.5$) of the Movchan-Demchishin-Thornton structure-zone model (*45*). The zone 2 is categorized as a columnar-like microstructure with well-defined metallurgical GBs (*45*), exactly as the Cr_2AlC MAX phase films obtained in this work and as shown in the detailed microstructural characterization presented in Figs. 1 and 2. In case of nanocrystallinity, this is also a result of fast cooling from vapor to solid phase during sputtering of atoms from the target toward the substrate.

The detection of amorphous nano-zones, accompanied by the low crystallinity observed from the x-ray diffractograms, indicates that the crystallization of the stoichiometric Cr_2AlC phase is not continuous at 648 K. As measured via STEM-EDX, the elemental composition of amorphous nano-zones is identical to the MAX phase, and this suggests that crystallization is only a matter to local

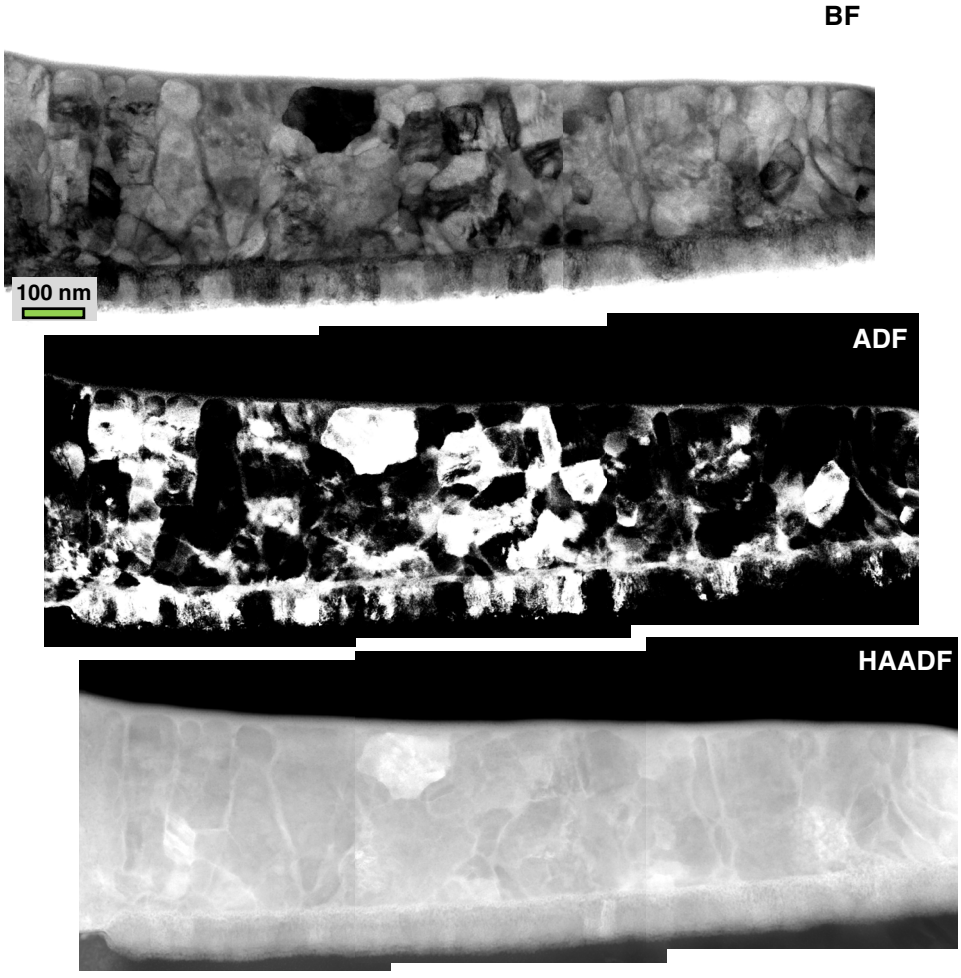

Fig. 6. Preserved nanocrystallinity after high-dose irradiation. Set of BF, ADF, and HAADF STEM micrographs showing an overview of the material after irradiation up to 40 dpa. The dual-phase Cr_2AlC coating had its nanocrystallinity preserved after high-dose heavy ion irradiation.

activation energies, and the crystallization can take place without (long-range) solid-state diffusion. The observed incomplete crystallization is rather associated with kinetic restrictions than non-stoichiometric conditions.

While the results obtained from XRD and TEM are in good agreement with each other, the inherent differences of these methods have to be kept in mind. First, the information direction in XRD is out of plane, whereas the one in TEM is in plane. Second, the information volume probed in XRD is significantly higher in comparison to that in TEM. Taking into account the high background and large peak broadening, it cannot be entirely excluded that the presence of minor phases is overlooked in the XRD pattern.

At first glance, the presence of amorphous nano-zones could act as preferential sites for nucleation of cracks in the material [nanostructured materials are known to offer good fracture resistance (*47*)], which could diminish its applicability in extreme environments. In its amorphous state, Cr_2AlC has higher free volume than in its MAX phase form. As introduced by Barenblatt (*48*), the modulus of cohesive forces is proportional to the distance between the atoms in a solid. Higher free volume implies higher distances between Cr, Al, and C atoms, thus resulting in reduced cohesion: This would favor the nucleation of cracks either under load or irradiation. However, as experimentally assessed using the nano-impact test (Fig. 7), the synthesized material exhibits an indentation behavior resembling to a ductile material, i.e., neither delamination nor cracks were observed after dynamic loading. These present results also agree with a recent detailed nano-indentation study performed by some of the present authors in the same material (*30*).

Radiation response of the dual-phase Cr_2AlC coating under extreme conditions

The first major experimental observation that can be made analyzing the heavy ion irradiation of the dual-phase Cr_2AlC coating is that the material has a high degree of phase stability at very high doses, i.e., 40 dpa or a fluence of 1.0×10^{16} ions cm^{-2}. This was confirmed by monitoring the SAED patterns of the irradiated area as a function of dose, as shown in the set of micrographs in Fig. 3 (E to H). The SAED pattern after irradiation up to 40 dpa (Fig. 3H) resembles the SAED pattern of the pristine material (Fig. 3E), and both nanocrystallinity and amorphous nano-regions (due to the presence of a central amorphous ring in the SAED pattern) remain after irradiation as the major characteristics of the dual-phase Cr_2AlC coating.

The high phase stability of the dual-phase Cr_2AlC coating up to 40 dpa can be understood when reports from literature on materials

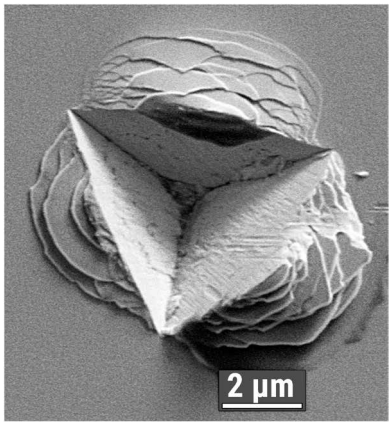

Fig. 7. Nano-impact testing of the dual-phase nanocrystalline Cr_2AlC MAX phase. Secondary electron micrograph showing the material after the nano-impact test. Although hard and with amorphous nano-zones, the material was not subjected to catastrophic failure.

degradation under energetic displacive environments are taken into consideration. Austenitic stainless steels—considered as conventional nuclear materials—are reported to undergo radiation-enhanced precipitation (REP) of $M_{23}C_6$ (known as τ-carbide) at doses around 20 dpa at 653 K (*49*) or radiation-induced precipitation (RIP) of the G phase around 11 dpa at 773 K (*50*) in neutron research reactors. In fast dose rates using particle accelerators, the dose levels for REP and RIP in austenitic stainless steels can be significantly lower. On the other hand, for potential nuclear materials, FeCr steels were reported to degrade around 2.5 dpa at 573 K where α′-phase precipitates were observed to form. Precipitation of the α′ phase in model FeCrAl alloys—promising candidate alloy selected by the U.S. Department of Energy to replace Zr alloys in future accident tolerant fuels (*51*)—has been reported to occur around 7 dpa at 593 K (*52*). All these materials degradation occur under dose levels below the requirements for future efficient nuclear reactors: 80 to 200 dpa (*53*). In addition, the most recent report on neutron irradiation of Ti-based MAX phases, Ti_3SiC_2 and Ti_2AlC, has shown that both materials are subjected to phase decomposition and radiation-induced segregation at 10 dpa (*17*).

A particular radiation effect detected in the dual-phase Cr_2AlC coating as a function of dose was the "thickening" of the columnar GBs, which was observed to occur as a function of dose, but clearer at the end of irradiation at 40 dpa as shown in the BFTEM micrograph in Fig. 3D. Figure 4 indicates that such thickening effect is related with both segregations of Cr and depletion of Al along the GBs. This effect can be observed in real time in the in situ TEM ion irradiation video provided as supplementary material. A similar effect was observed to occur in TiN nanocrystalline thin films when subjected to 134-keV Xe ion irradiation (*27*). The STEM-EDX analysis shown in Fig. 4 also indicates the presence of Xe bubbles, which was expected given the bombardment conditions, throughout the microstructure of the dual-phase Cr_2AlC coating. The bubbles were noticeably larger in size along the GBs. No apparent change was noticeable in the C maps, suggesting that the X layers remained unaffected by the irradiation. The segregation of Cr along the nanocrystalline GBs acts to impede any grain growth or swelling as a result of the irradiation, therefore stabilizing the nanocrystalline microstructure of the Cr2AlC coating under irradiation.

Unveiling the mechanisms of swelling and radiation resistance of the dual-phase Cr_2AlC coating

The nucleation and growth of inert gas bubbles in solids manifest itself in a phenomenon known as swelling (*54*). To investigate in depth the swelling effects caused by Xe irradiation in the present coating material, STEM-EDX was performed at a higher magnification, revealing that the Xe bubbles are bigger along the GBs when compared with the matrix as shown in Fig. 5 (A to F). This EDX mapping also reveals Cr segregation and dealumination along the GBs.

The results mentioned in the paragraph above indicate a possible connection between Cr segregation and Xe bubble growth and Cr segregation. The micrograph in Fig. 5G reveals the synergistic relationship between the swelling (created by a Xe bubble) and the interfacial thickening phenomena. It has been found that upon nucleation and growth, Xe bubbles induce the segregation of the M-layer element Cr, which presents a trend for either formation of nanometer-size clusters or segregation toward the GBs.

These experimental results indicate that the radiation-induced segregation effect observed in this work may be (solely) a consequence of the extreme Xe implantation yield (i.e., high fluence). Inert gases have low solubility in solids (*55*). Thus, upon continuous irradiation, the accumulation of Xe within the dual-phase Cr_2AlC coating will inevitably lead to the formation of Xe bubbles that upon growth will cause the segregation of Cr along the GBs. Therefore, in a neutron environment without a significant yield of transmutation from Cr, Al, and C to inert gases [e.g., transmutation yield of Cr and Al to He is around 80 to 300 atomic parts per million $year^{-1}$ (*56*)], such radiation-induced segregation phenomenon will likely not occur. The produced material can be considered a promising candidate for further research in material test reactors.

Another experimental observation that deserves further attention is the detection of larger Xe bubbles along the GBs. Using the Xe elemental maps and the software ImageJ for particle analysis, the size quantification of Xe bubbles at trans- and intragranular positions indicate that the average sizes of bubbles are respectively 1.83 ± 0.04 and 3.06 ± 0.06 nm. It is worth emphasizing that these values are significantly lower than Xe bubbles in the microstructure of Xe irradiated (under similar conditions) TiN coatings, which are around 25 nm at doses as low as 6.2 dpa (*27*). This observation indicates that nanocrystallinity is a key parameter in the radiation response of the dual-phase Cr_2AlC coating because of the following reasons. The theory of inert gas bubbles in solids shows that bubbles can grow not only upon coalescence but also upon incorporation of vacancies and Xe interstitials diffusing at seed bubbles (*54*, *57*, *58*). As Xe bubbles are observed to be larger at intragranular positions, this suggests that GBs are specific site dependencies acting as preferential sinks for point defects induced by irradiation. This is also a trend recently observed in the scientific literature (*59*). However, the reported results herein indicate that Xe bubbles can be used as a track to detect the efficiency of sinks in a complex model material such as the dual-phase nanocrystalline Cr_2AlC coating.

It is also expected that the amorphous nano-regions act actively to sink radiation-induced point defects due to the free volume of these zones compared with crystalline regions of the material. This suggests that the nano-amorphous phases can also accommodate diffusing point defects and act as nucleation sites for bubbles and Cr segregation.

Why no complete amorphization is observed after irradiation given the preexistence of amorphous nano-regions

It is well established within the field of nuclear materials that ceramics (*22*), minerals (*60*–*62*), and semiconductors (*63*–*65*) are classes of crystalline solids that incur amorphization under irradiation. Amorphization occurs under irradiation when the atomic collisions induce accumulation of crystalline defects to supersaturated levels, thus locally destroying the long-range order (LRO) symmetry of the crystalline solid (*61*). Microstructurally, the loss of LRO creates amorphous nano-regions that upon overlapping will induce the complete amorphization state, i.e., the complete collapse of the initial crystalline structure. It has been extensively reported in literature that for nuclear-grade ceramics such as SiC under Xe irradiation, the amorphization threshold dose within the temperature range of 50 to 450 K falls below 1 dpa (the heavier the ion, the lower the amorphization threshold dose) (*22*). In the case of minerals like zircon, continuous natural irradiation from α-decay of U and Th impurities can induce the occurrence of amorphous nano-zones at around 0.4 dpa, which eventually overlap upon growth to completely amorphize the material at around 0.8 dpa (*60*).

A counterintuitive result was obtained when irradiating the dual-phase Cr_2AlC in this work: The preexistence of amorphous nano-zones has not induced the complete amorphization of the coating structure. This result suggests that the nanocrystallinity of the synthesized material as well as the secondary amorphous nanophases via free volume are contributing to mitigate the accumulation of displacement damage defects, preventing amorphization. This can be interpreted as a "self-healing capability" of the "nonpure" MAX phase under extreme environments, suggesting that the behavior under irradiation of Cr-based MAX phases is different from conventional nuclear-grade ceramics.

As recently reviewed by Zhang and Weber (*66*), there are some cases in which energetic particle irradiation does not damage the structure of materials: Conversely, it can even induce annealing of preexisting defects. When high-energy ions are used [often for energies higher than 1 MeV (*66*)], the dominance of electronic energy dissipation may result in ionization-induced annealing (IIA), which can act to mitigate the accumulation of radiation damage within crystalline structures or even preventing amorphization in ceramics (*67*). For the irradiation conditions reported in this work, the non-amorphization of the studied material under irradiation is likely rather associated with its inherent nanocrystallinity than the IIA phenomenon: If the latter occurred, it was not sufficient to prevent the formation of Xe bubbles and radiation-induced segregation and clustering as both are manifestation of radiation damage arising from the generation of defects in excess concentrations.

The question of whether this material in its bulk form can sustain high doses of radiation without complete amorphization is a motivation for future work. However, the presence of nanocrystalline grains and large number of GBs will help the material to prevent the accumulation of irradiation-induced defects. Therefore, the results reported in this work indicate that the mixed crystalline Cr_2AlC thin film along with amorphous nano-zones (thus, deviating from the pure MAX phase concept) ought to be treated as a potential candidate to be a structural material for the next generation of nuclear reactors.

The technology of accident tolerant fuels and potential nuclear materials for future fission and fusion nuclear power plants requires the ability of their crystalline structure to sustain phase stability up to extremely high doses. However, the behavior of most conventional nuclear materials remains tied in the upper limit of such extreme dose levels.

The radiation response of model dual-phase Cr_2AlC coating herein was investigated using in situ TEM heavy ion irradiation and state-of-the-art electron microscopy characterization techniques. It was demonstrated that using magnetron sputtering with a specific set of deposition parameters, the final coating can be engineered at nanoscale to generate a dual-phase material that comprises a major Cr_2AlC MAX phase along with amorphous nano-regions with similar atomic composition. The major advantage of using this synthesis technique—compared with existing bulk methodologies—is that the material can be produced at lower deposition temperatures, posing no significant metallurgical changes to the substrate material. In addition, nano-impact testing suggests that the synthesized material may not suffer catastrophic fracture under dynamic loading conditions, indicating that the presence of amorphous nano-zones may have a negligible impact on the fracture resistance and then in the overall toughness of the coating.

Heavy ion irradiation up to extreme doses of 40 dpa revealed that the material holds its initial matrix phase intact after irradiation. A major discovery made in the present work is that Xe bubbles, upon growth, synergistically induce the observed radiation-induced segregation of Cr. A direct association between swelling and radiation-induced segregation was obtained here: Upon growth of bubbles, the MAX phase degradation starts in the M layers with the formation of Cr clusters at the surroundings of the Xe bubbles. Therefore, the degradation observed herein is limited to the fact that the Xe irradiation induces a large yield of Xe atoms to be implanted in the material, allowing the growth of bubbles, thus inducing the subsequent segregation. It is expected that this material does not suffer significant (if any) transmutation to inert gases in a neutron environment.

Xe irradiation was also used to tackle the assumption that a nanocrystalline material has efficient and active-site sinks for point-induced radiation effects. It was found that Xe bubbles are bigger along the GBs, suggesting that a coating for energetic displacive environments can benefit from nanocrystallinity. In addition, the presence of amorphous nano-zones contributes for such enhanced radiation resistance as they are also active sites for defect sinking, thus deviating from the initial concept of a fully crystalline MAX phase for energetic particle environments.

The importance of the present study can be better understood considering previously reported Cr_2AlC material properties. Cr_2AlC can be easily deposited on industrial scale and onto large surfaces by physical vapor deposition techniques in the amorphous state. The material can then be crystallized by high-temperature annealing without any detrimental effects. It has been shown that under LWR's conditions, the crystalline material is both stable in the pressurized water at elevated temperatures and radiation tolerant. Here, we demonstrated that if recrystallization from an amorphous state is not fully attained, the material also exhibits high radiation tolerance. In addition, this work also emphasizes that the nanocrystalline form of Cr_2AlC is stable to local chemical variations, which is technologically very significative. The radiation response of the dual-phase Cr_2AlC material reported herein allows to predict the effect of irradiation in the material in its fully amorphous condition; therefore, this work paves the way for the use of Cr_2AlC coatings in extreme environments in any available solid-state structure.

The fact that the dual-phase Cr_2AlC coating material can be produced in an engineering-industrial scale using deposition techniques makes it an attractive candidate material for the future generation of fission and fusion nuclear power plants. It is important to emphasize that the material studied herein was under prototypic conditions; therefore, when considering the material to be applied in nuclear reactors, the compatibility with different substrates, metallic claddings, and with the coolant material (e.g., corrosion, oxidation resistances, and realistic neutron irradiation spectrum) must be addressed in future research. We appreciate that all ion irradiations somehow are different from neutron irradiation. The ion irradiation is a valuable step before more laborious neutron irradiation trials.

MATERIALS AND METHODS

Synthesis of Cr-Al-C coatings and TEM sample preparation

Thin solid films from the Cr-Al-C ternary system were synthesized using magnetron-sputtering deposition. The deposition was performed from Cr, Al, and C elemental targets with 6.35 cm (99.99% purity) that were positioned in the central volume of the deposition chamber. The deposition was carried out using a layer-by-layer method reported earlier (*68*). The films were deposited onto electronic-grade Si (100) substrates. The deposition temperature was monitored with a thermocouple to be constant at 648 K. After deposition, electron-transparent specimens were prepared using the focused ion beam conventional lift-out technique in a FEI Quanta 200 three-dimensional dual-beam scanning electron microscope operating a 30-keV Ga^+ ion source (*69*). The surfaces of samples were protected with a 3-μm-thick Pt layer to avoid sputtering and damage from the ion source.

X-ray diffraction

XRD data were acquired with a Bruker ASX Advance D8 diffractometer operating with Cu K_α radiation, which allowed to study the crystallographic structure of the coating in as-deposited state. The measurement was performed in grazing incidence geometry at an incidence angle of 1°.

In situ TEM irradiation and annealing

Electron-transparent specimens were subjected to in situ TEM heavy ion irradiations at the MIAMI-2 facility (*70*). The facility consists of a 350-keV National Electrostatics Corporation ion source coupled with a Hitachi H-9500 TEM operating at 300 keV. An ion beam of Xe^+ with 300 keV was selected to provide radiation damage to assess both atomic displacements and implantation aiming at analyzing the nucleation and growth of inert gas bubbles within the films. These conditions simulate those experienced within the operational setup of a conventional LWR. The ion flux measured at the specimen position was 2×10^{13} ions cm^{-2} per second, and the specimens were heated up to 623 K by using a Gatan double-tilt heating holder (Ta-made furnace) and held at this temperature during the irradiation experiments. Under these irradiation conditions, the maximum achieved fluence was 1.0×10^{16} ions cm^{-2}.

SRIM-2013Pro was used for calculating the fluence to dpa using the full-damage cascade model according to (*71*). The dpa was calculated assuming a specimen thickness of 150 nm, average atomic density of 8.9×10^{22} atoms cm^{-3}, and displacement energies were set to 40 eV for Cr, Al, and C (*72*). This yields to an average of 40-dpa peak when the fluence is 1.0×10^{16} ions cm^{-2}. It is important to emphasize that per one ion collision, SRIM predicts the generation of 2580 vacancies. Detailed information on the fluence-to-dose calculations is provided in the Supplementary Materials.

Electron microscopy characterization and postirradiation methodology

Pre-irradiated and post-irradiated specimens were further characterized in the Hitachi H-9500 at the MIAMI facility and at the Montanuniversitaet Leoben by using a Thermo Fisher Scientific Talos F200X STEM operating a field-emission gun at 200 keV. Super-X EDX spectroscopy was used for either elemental mapping or estimating the elemental composition of the studied materials. Before the investigations within the electron microscopes, the specimens were plasma-cleaned within Ar atmosphere for 20 min using a Diener Femto plasma cleaner to avoid contamination of carbonaceous material particularly during the STEM measurements. It has been found that 20 min of plasma cleaning significantly reduces C uptake during EDX measurements. Electron microscopy micrographs were further analyzed with the ImageJ, Velox, and Gatan Microscopy Suite software. Quantitative data, such as the bubble sizes, were processed using DataGraph in combination with ImageJ. Elemental composition quantification has been carried out with EDX data within the Velox software using a multipolynomial model with parabolic background removal and a density of 5.23 g cm^{-3} (Cr_2AlC). For the EDX quantification, Bote-Salvat approximation was used as the ionization cross-sectional model.

Nano-impact testing

Micro Materials Ltd. nanomechanical platform 3 was used to assess the mechanical behavior of the dual-phase nanocrystalline Cr_2AlC coating via nano-impact testing. The tests were undertaken with a blunt Berkovich nanoindenter as impactor at room temperature. Further details on nano-impact testing are described elsewhere (*40*).

SUPPLEMENTARY MATERIALS

Supplementary material for this article is available at http://advances.sciencemag.org/cgi/content/full/7/13/eabf6771/DC1

REFERENCES AND NOTES

1. A. C. D. Chaklader, "Reactive hot pressing": A new ceramic process. *Nature* **206**, 392–393 (1965).
2. W. Jeitschko, H. Nowotny, Die Kristallstruktur von Ti_3SiC_2—Ein neuer Komplexcarbid-Typ. *Monatshefte für Chemie.* **98**, 329–337 (1967).
3. M. W. Barsoum, T. El-Raghy, The MAX phases: Unique new carbide and nitride materials: Tertiary ceramics are soft and machinable, yet heat-tolerant, strong and lighweight. *Am. Sci.* **89**, 334–343 (2001).
4. J. Morgiel, J. Lis, R. Pampuch, Microstructure of Ti_3SiC_2-based ceramics. *Mater. Lett.* **27**, 85–89 (1996).
5. J. Gruber, A. C. Lang, J. Griggs, M. L. Taheri, G. J. Tucker, M. W. Barsoum, Evidence for bulk ripplocations in layered solids. *Sci. Rep.* **6**, 33451 (2016).
6. Z. Lin, M. Li, J. Wang, Y. Zhou, Microstructure and high-temperature corrosion behavior of a Cr-Al-C composite. *J. Am. Ceram. Soc.* **90**, 3930–3937 (2007).
7. V. D. Jovic, B. M. Jovic, S. Gupta, T. El-Raghy, M. W. Barsoum, Corrosion behavior of select MAX phases in NaOH, HCl and H_2SO_4. *Corros. Sci.* **48**, 4274–4282 (2006).
8. E. N. Hoffman, D. W. Vinson, R. L. Sindelar, D. J. Tallman, G. Kohse, M. W. Barsoum, MAX phase carbides and nitrides: Properties for future nuclear power plant in-core applications and neutron transmutation analysis. *Nucl. Eng. Des.* **244**, 17–24 (2012).
9. M. W. Barsoum, The $M_{N+1}AX_N$ phases: A new class of solids: Thermodynamically stable nanolaminates. *Prog. Solid State Chem.* **28**, 201–281 (2000).
10. J. Lis, Y. Miyamoto, R. Pampuch, K. Tanihata, Ti_3SiC-based materials prepared by HIP-SHS techniques. *Mater. Lett.* **22**, 163–168 (1995).

11. J. Lis, R. Pampuch, J. Piekarczyk, L. Stobierski, New ceramics based on Ti_3SiC_2. *Ceram. Int.* **19**, 219–222 (1993).
12. M. Sundberg, G. Malmqvist, A. Magnusson, T. El-Raghy, in *Ceramics International* (Elsevier, 2004), vol. 30, pp. 1899–1904; https://sciencedirect.com/science/article/pii/S0272884204001245.
13. C. Wang, C. L. Tracy, R. C. Ewing, Radiation effects in $M_{n+1A}X_n$ phases. *Appl. Phys. Rev.* **7**, 41311 (2020).
14. D. J. Tallman, L. He, J. Gan, E. N. Caspi, E. N. Hoffman, M. W. Barsoum, Effects of neutron irradiation of Ti_3SiC_2 and Ti_3AlC_2 in the 121–1085 °C temperature range. *J. Nucl. Mater.* **484**, 120–134 (2017).
15. D. J. Tallman, E. N. Hoffman, E. N. Caspi, B. L. Garcia-Diaz, G. Kohse, R. L. Sindelar, M. W. Barsoum, Effect of neutron irradiation on select MAX phases. *Acta Mater.* **85**, 132–143 (2015).
16. D. J. Tallman, L. He, B. L. Garcia-Diaz, E. N. Hoffman, G. Kohse, R. L. Sindelar, M. W. Barsoum, Effect of neutron irradiation on defect evolution in Ti_3SiC_2 and Ti_2AlC. *J. Nucl. Mater.* **468**, 194–206 (2016).
17. M. A. Tunes, R. W. Harrison, S. E. Donnelly, P. D. Edmondson, A transmission electron microscopy study of the neutron-irradiation response of Ti-based MAX phases at high temperatures. *Acta Mater.* **169**, 237–247 (2019).
18. D. W. Clark, S. J. Zinkle, M. K. Patel, C. M. Parish, High temperature ion irradiation effects in MAX phase ceramics. *Acta Mater.* **105**, 130–146 (2016).
19. K. R. Whittle, M. G. Blackford, R. D. Aughterson, S. Moricca, G. R. Lumpkin, D. P. Riley, N. J. Zaluzec, Radiation tolerance of $M_{n+1}AX_n$ phases, Ti_3AlC_2 and Ti_3SiC_2. *Acta Mater.* **58**, 4362–4368 (2010).
20. L. Zhang, Q. Qi, L. Q. Shi, D. J. O'Connor, B. V. King, E. H. Kisi, D. K. Venkatachalam, Damage tolerance of Ti_3SiC_2 to high energy iodine irradiation. *Appl. Surf. Sci.* **258**, 6281–6287 (2012).
21. C. Wang, T. Yang, S. Kong, J. Xiao, J. Xue, Q. Wang, C. Hu, Q. Huang, Y. Wang, Effects of He irradiation on Ti_3AlC_2: Damage evolution and behavior of He bubbles. *J. Nucl. Mater.* **440**, 606–611 (2013).
22. S. J. Zinkle, L. L. Snead, Influence of irradiation spectrum and implanted ions on the amorphization of ceramics. *Nucl. Instrum. Methods Phys. Res. B* **116**, 92–101 (1996).
23. J. Ward, S. Middleburgh, M. Topping, A. Garner, D. Stewart, M. W. Barsoum, M. Preuss, P. Frankel, Crystallographic evolution of MAX phases in proton irradiating environments. *J. Nucl. Mater.* **502**, 220–227 (2018).
24. J. Ward, D. Bowden, D. Stewart, M. W. Barsoum, P. Frankel, M. Preuss, Influence of proton-irradiation temperature on the damage accumulation in Ti_3SiC_2 and Ti_3AlC_2. *Scr. Mater.* **165**, 98–102 (2019).
25. C. Walter, D. P. Sigumonrong, T. El-Raghy, J. M. Schneider, Towards large area deposition of Cr_2AlC on steel. *Thin Solid Films* **515**, 389–393 (2006).
26. V. Vishnyakov, O. Crisan, P. Dobrosz, J. S. Colligon, Ion sputter-deposition and in-air crystallisation of Cr_2AlC films. *Vacuum* **100**, 61–65 (2014).
27. M. A. Tunes, F. C. da Silva, O. Camara, C. G. Schön, J. C. Sagás, L. C. Fontana, S. E. Donnelly, G. Greaves, P. D. Edmondson, Energetic particle irradiation study of TiN coatings: Are these films appropriate for accident tolerant fuels? *J. Nucl. Mater.* **512**, 239–245 (2018).
28. M. A. Tunes, V. M. Vishnyakov, O. Camara, G. Greaves, P. D. Edmondson, Y. Zhang, S. E. Donnelly, A candidate accident tolerant fuel system based on a highly concentrated alloy thin film. *Mater. Today Energy* **12**, 356–362 (2019).
29. J. Ward, D. Bowden, E. Prestat, S. Holdsworth, D. Stewart, M. W. Barsoum, M. Preuss, P. Frankel, Corrosion performance of Ti_3SiC_2, Ti_3AlC_2, Ti_2AlC and Cr_2AlC MAX phases in simulated primary water conditions. *Corros. Sci.* **139**, 444–453 (2018).
30. M. Imtyazuddin, A. H. Mir, M. A. Tunes, V. M. Vishnyakov, Radiation resistance and mechanical properties of magnetron-sputtered Cr_2AlC thin films. *J. Nucl. Mater.* **526**, 151742 (2019).
31. C. Wang, Z. Han, R. Su, J. Gao, L. Shi, Effects of irradiation damage on the structure in Cr_2AlC thin film. *Nucl. Instrum. Methods Phys. Res. B* **450**, 286–290 (2019).
32. Q. Huang, H. Han, R. Liu, G. Lei, L. Yan, J. Zhou, Q. Huang, Saturation of ion irradiation effects in MAX phase Cr_2AlC. *Acta Mater.* **110**, 1–7 (2016).
33. C. Wang, T. Yang, J. Xiao, S. Liu, J. Xue, Q. Huang, J. Zhang, J. Wang, Y. Wang, Structural transitions induced by ion irradiation in V_2AlC and Cr_2AlC. *J. Am. Ceram. Soc.* **99**, 1769–1777 (2016).
34. M. Bugnet, V. Mauchamp, E. Oliviero, M. Jaouen, T. Cabioc'h, Chemically sensitive amorphization process in the nanolaminated Cr_2AC (A = Al or Ge) system from TEM in situ irradiation. *J. Nucl. Mater.* **441**, 133–137 (2013).
35. C. Wang, H. Tu, R. Su, J. Gao, B. V. King, D. J. O'Connor, L. Shi, Annealing effects on the structure and hardness of helium-irradiated Cr_2AlC thin films. *J. Am. Ceram. Soc.* **104**, 593–603 (2021).
36. M. Imtyazuddin, A. H. Mir, E. Aradi, V. Vishnyakov, Effect of aluminium concentration on phase formation and radiation stability of Cr_2Al_xC thin film. *Nanotechnology* **31**, 385602 (2020).
37. International Centre for Diffraction Data, "Cr2AlC crystallographic data for XRD: Card number 00-029-0017" (2020).
38. B. D. Beake, V. M. Vishnyakov, J. S. Colligon, Nano-impact testing of TiFeN and TiFeMoN films for dynamic toughness evaluation. *J. Phys. D Appl. Phys.* **44**, 085301 (2011).
39. X. Shi, H. Li, B. D. Beake, M. Bao, T. W. Liskiewicz, Z. Sun, J. Chen, Dynamic fracture of CrN coating by highly-resolved nano-impact. *Surf. Coatings Technol.* **383**, 125288 (2020).
40. B. D. Beake, S. R. Goodes, J. F. Smith, Micro-impact testing: A new technique for investigating thin film toughness, adhesion, erosive wear resistance, and dynamic hardness. *Surf. Eng.* **17**, 187–192 (2001).
41. J. J. Li, L. F. Hu, F. Z. Li, M. S. Li, Y. C. Zhou, Variation of microstructure and composition of the Cr_2AlC coating prepared by sputtering at 370 and 500 °C. *Surf. Coatings Technol.* **204**, 3838–3845 (2010).
42. A. Abdulkadhim, M. to Baben, T. Takahashi, V. Schnabel, M. Hans, C. Polzer, P. Polcik, J. M. Schneider, Crystallization kinetics of amorphous Cr_2AlC thin films. *Surf. Coatings Technol.* **206**, 599–603 (2011).
43. J. M. Schneider, Z. Sun, R. Mertens, F. Uestel, R. Ahuja, Ab initio calculations and experimental determination of the structure of Cr_2AlC. *Solid State Commun.* **130**, 445–449 (2004).
44. W.-B. Tian, P.-L. Wang, Y.-M. Kan, G.-J. Zhang, Y.-X. Li, D.-S. Yan, Phase formation sequence of Cr_2AlC ceramics starting from Cr–Al–C powders. *Mater. Sci. Eng. A* **443**, 229–234 (2007).
45. J. A. Thornton, The microstructure of sputter-deposited coatings. *J. Vac. Sci. Technol. A* **4**, 3059–3065 (1986).
46. L.-O. Xiao, S.-B. Li, G. Song, W. G. Sloof, Synthesis and thermal stability of Cr_2AlC. *J. Eur. Ceram. Soc.* **31**, 1497–1502 (2011).
47. C. Mitterer, P. H. Mayrhofer, M. Beschliesser, P. Losbichler, P. Warbichler, F. Hofer, P. N. Gibson, W. Gissler, H. Hruby, J. Musil, J. Vlček, in *Surface and Coatings Technology* (1999), vols. 120–121, pp. 405–411.
48. G. I. Barenblatt, The mathematical theory of equilibrium cracks in brittle fracture. *Adv. Appl. Mech.* **7**, 55–129 (1962).
49. P. J. Maziasz, Formation and stability of radiation-induced phases in neutron-irradiated austenitic and ferritic steels. *J. Nucl. Mater.* **169**, 95–115 (1989).
50. F. A. Garner, in *Comprehensive Nuclear Materials* (Elsevier, 2012), vol. 4, pp. 33–95.
51. R. B. Rebak, K. A. Terrani, W. P. Gassmann, J. B. Williams, K. L. Ledford, Improving nuclear power plant safety with FeCrAl alloy fuel cladding. *MRS Adv.* **2**, 1217–1224 (2017).
52. S. A. Briggs, P. D. Edmondson, K. C. Littrell, Y. Yamamoto, R. H. Howard, C. R. Daily, K. A. Terrani, K. Sridharan, K. G. Field, A combined APT and SANS investigation of α′ phase precipitation in neutron-irradiated model FeCrAl alloys. *Acta Mater.* **129**, 217–228 (2017).
53. S. J. Zinkle, G. S. Was, Materials challenges in nuclear energy. *Acta Mater.* **61**, 735–758 (2013).
54. S. E. Donnelly, The density and pressure of helium in bubbles in implanted metals: A critical review. *Radiat. Eff.* **90**, 1–47 (1985).
55. A. H. Mir, J. A. Hinks, J.-M. Delaye, S. Peuget, S. E. Donnelly, Xenon solubility and formation of supercritical xenon precipitates in glasses under non-equilibrium conditions. *Sci. Rep.* **8**, 15320 (2018).
56. M. R. Gilbert, J.-C. Sublet, R. A. Forrest, Handbook of activation, transmutation, and radiation damage properties of the elements simulated using FISPACT-II & TENDL-2014; Magnetic Fusion Plants, *Ccfe-R(15)26* (2015), pp. 1–696.
57. R. S. Barnes, A theory of swelling and gas release for reactor materials. *J. Nucl. Mater.* **11**, 135–148 (1964).
58. M. W. Thompson, *Defects and Radiation Damage in Metals* (Cambridge Univ. Press, 1969).
59. O. El-Atwani, N. Li, M. Li, A. Devaraj, J. K. S. Baldwin, M. M. Schneider, D. Sobieraj, J. S. Wróbel, D. Nguyen-Manh, S. A. Maloy, E. Martinez, Outstanding radiation resistance of tungsten-based high-entropy alloys. *Sci. Adv.* **5**, eaav2002 (2019).
60. B. C. Chakoumakos, T. Murakami, G. R. Lumpkin, R. C. Ewing, Alpha-decay–induced fracturing in zircon: The transition from the crystalline to the metamict state. *Science* **236**, 1556–1559 (1987).
61. W. J. Weber, R. C. Ewing, L. M. Wang, The radiation-induced crystalline-to-amorphous transition in zircon. *J. Mater. Res.* **9**, 688–698 (1994).
62. L. Nasdala, M. Wenzel, G. Vavra, G. Irmer, T. Wenzel, B. Kober, Metamictisation of natural zircon: Accumulaton versus thermal annealing of radioactivity-induced damage. *Contrib. Mineral. Petrol.* **141**, 125–144 (2001).
63. P. D. Edmondson, K. J. Abrams, J. A. Hinks, G. Greaves, C. J. Pawley, I. Hanif, S. E. Donnelly, An in situ transmission electron microscopy study of the ion irradiation induced amorphisation of silicon by He and Xe. *Scr. Mater.* **113**, 190–193 (2016).
64. J. S. Williams, X. Zhu, M. C. Ridgway, M. J. Conway, B. C. Williams, F. Fortuna, M. O. Ruault, H. Bernas, Preferential amorphization and defect annihilation at nanocavities in silicon during ion irradiation. *Appl. Phys. Lett.* **77**, 4280–4282 (2000).
65. O. Camara, M. A. Tunes, G. Greaves, A. H. Mir, S. Donnelly, J. A. Hinks, Understanding amorphization mechanisms using ion irradiation in situ a TEM and 3D damage reconstruction. *Ultramicroscopy* **207**, 112838 (2019).
66. Y. Zhang, W. J. Weber, Ion irradiation and modification: The role of coupled electronic and nuclear energy dissipation and subsequent nonequilibrium processes in materials. *Appl. Phys. Rev.* **7**, 041307 (2020).
67. Y. Zhang, H. Xue, E. Zarkadoula, R. Sachan, C. Ostrouchov, P. Liu, X.-I. Wang, S. Zhang, T. S. Wang, W. J. Weber, Coupled electronic and atomic effects on defect evolution in silicon carbide under ion irradiation. *Curr. Opin. Solid State Mater. Sci.* **21**, 285–298 (2017).

68. V. Vishnyakov, J. Lu, P. Eklund, L. Hultman, J. Colligon, Ti_3SiC_2-formation during Ti–C–Si multilayer deposition by magnetron sputtering at 650 °C. *Vacuum* **93**, 56–59 (2013).
69. L. A. Giannuzzi, F. A. Stevie, A review of focused ion beam milling techniques for TEM specimen preparation. *Micron* **30**, 197–204 (1999).
70. G. Greaves, A. H. Mir, R. W. Harrison, M. A. Tunes, S. E. Donnelly, J. A. Hinks, New Microscope and Ion Accelerators for Materials Investigations (MIAMI-2) system at the University of Huddersfield. *Nucl. Instrum. Methods Phys. Res. A* **931**, 37–43 (2019).
71. W. J. Weber, Y. Zhang, Predicting damage production in monoatomic and multi-elemental targets using stopping and range of ions in matter code: Challenges and recommendations. *Curr. Opin. Solid State Mater. Sci.* **23**, 100757 (2019).
72. R. E. Stoller, M. B. Toloczko, G. S. Was, A. G. Certain, S. Dwaraknath, F. A. Garner, On the use of SRIM for computing radiation damage exposure. *Nucl. Instrum. Methods Phys. Res. B* **310**, 75–80 (2013).

Acknowledgments: M.A.T., M.I., and V.M.V. would like to thank G. Greaves and A. H. Mir at the University of Huddersfield for assistance with past experiments. M.A.T. and V.M.V. would like to thank U. Jansson (Uppsala University) for the idea to perform XRD on the pristine samples. V.M.V. is grateful to A. Harris (Micro Materials Ltd.) for assistance with nano-impact testing. M.A.T. is grateful to C. G. Schön (University of São Paulo) for the discussion on Barenblatt's fracture mechanics work. **Funding:** M.A.T. and S.P. are grateful to the European Research Council (ERC) excellent science grant "TRANSDESIGN" through the Horizon 2020 program under contract 757961 and by the financial support from the Austrian Research Promotion Agency (FFG) in the project 3D nanoAnalytics (FFG-No 858040). M.I. and V.M.V. are grateful to the Engineering and Physical Sciences Research Council (EPRSC) for funding MIAMI facilities under the grants EP/E017266/1 and EP/M028283/1. Funding for this research has also been provided by the Austrian Federal Ministry for Digital and Economic Affairs and the National Foundation for Research, Technology, and Development (CDL-ACCT). **Author contributions:** M.A.T. and M.I. performed the electron microscopy research including data acquisition and processing. M.I. and V.M.V. designed and synthesized the Cr_2AlC thin solid films. C.K. performed the XRD analysis. All the authors participated in the discussion and conceptualization of this research work including writing and editing the manuscript. V.M.V. and S.P. secured the funding for the research reported in this manuscript. **Competing interests:** The authors declare that they have no competing interests. **Data and materials availability:** All data needed to evaluate the conclusions in the paper are present in the paper and/or the Supplementary Materials. Raw data will be available upon request. Requests for materials should be addressed to the corresponding author M.A.T. (m.a.tunes@physics.org) or to V.M.V. (v.vishnyakov@hud.ac.uk).

Submitted 12 November 2020
Accepted 3 February 2021
Published 24 March 2021
10.1126/sciadv.abf6771

Citation: M. A. Tunes, M. Imtyazuddin, C. Kainz, S. Pogatscher, V. M. Vishnyakov, Deviating from the pure MAX phase concept: Radiation-tolerant nanostructured dual-phase Cr_2AlC. *Sci. Adv.* **7**, eabf6771 (2021).

ScienceAdvances

Deviating from the pure MAX phase concept: Radiation-tolerant nanostructured dual-phase CrAlC

M. A. TunesM. ImtyazuddinC. KainzS. PogatscherV.M. Vishnyakov

Sci. Adv., 7 (13), eabf6771. • DOI: 10.1126/sciadv.abf6771

Science Advances (ISSN 2375-2548) is published by the American Association for the Advancement of Science. 1200 New York Avenue NW, Washington, DC 20005. The title *Science Advances* is a registered trademark of AAAS.